PHYSICAL REVIEW D **76,** 094017 (2007)

Unified description of diffractive deep inelastic scattering with saturation

Cyrille Marquet*

RIKEN BNL Research Center, Brookhaven National Laboratory, Upton, New York 11973, USA

(Received 20 June 2007; published 15 November 2007)

We propose a new description of inclusive diffraction in deep inelastic scattering. The diffractive structure functions are expressed in the dipole picture and contain heavy-quark contributions. The dipole scattering amplitude, a saturation model fitted on inclusive deep inelastic scattering data, features a saturation scale $Q_s(x)$ larger than 1 GeV for $x = 10^{-5}$. The $q\bar{q}g$ contribution to the diffractive final state is modeled in such a way that both the large-Q^2 and small-β limits are implemented. In the regime $x_{\mathbb{P}} < 0.01$ in which saturation is expected to be relevant, we obtain a parameter-free description of the HERA data with $\chi^2/\text{points} = 1.2$.

DOI: 10.1103/PhysRevD.76.094017 PACS numbers: 13.60.Hb, 12.38.Bx

I. INTRODUCTION

Deep inelastic scattering (DIS) is a process in which a virtual photon is used as a hard probe to resolve the small distances inside a proton and study its partonic constituents: quarks and gluons that obey the laws of perturbative QCD. When probing with a fixed photon virtuality $Q^2 \gg \Lambda^2_{\text{QCD}}$, and increasing the energy of the photon-proton collision W, the parton densities seen by the photon inside the proton grow. Eventually, at some energy much bigger than the hard scale, corresponding to a small value of the Bjorken variable $x \simeq Q^2/W^2$, the gluon density probed becomes so large that nonlinear effects like gluon recombination become important. One enters a nonlinear yet weakly coupled regime of QCD [1] called the saturation regime.

The transition to the saturation regime is characterized by the so-called saturation momentum $Q_s(x) = Q_0 x^{-\lambda/2}$. This is an intrinsic scale of the high-energy proton which increases as x decreases. $Q_0 \sim \Lambda_{\text{QCD}}$, but as the energy increases, Q_s becomes a hard scale, and the transition to saturation occurs when Q_s becomes comparable to Q. The higher Q^2 is, the smaller x should be to enter the saturation regime. Part of the DIS events are diffractive, meaning that the proton remains intact after the collision and there is a rapidity gap between that proton and the rest of the final-state particles. Such events are expected to be more sensitive to the saturation regime than the inclusive ones.

Although the saturation regime is only reached when $Q_s \sim Q$, observables are sensitive to the saturation scale already during the approach to saturation [2] when $\Lambda_{\text{QCD}} \ll Q_s \ll Q$. For inclusive events in deep inelastic scattering, this feature manifests itself via the so-called geometric scaling property: instead of being a function of Q^2/Q_0^2 and x separately, the total cross section is only a function of $\tau = Q^2/Q_s^2(x)$, up to large values of τ. Experimental measurements of inclusive DIS are compatible with that prediction [3]. Recently, it was shown [4] that diffractive observables also feature the geometric scaling behaviors expected when approaching saturation.

In the saturation regime of QCD, contributions to the cross sections growing like Q_s/Q are important. The leading-twist approximation of perturbative QCD, in which Q^2 is taken as the biggest scale, cannot account for such contributions, and therefore is not appropriate to describe the small-x limit of deep inelastic scattering. As leading-twist gluon distributions cannot be used to compute cross sections, the dipole picture of DIS [5] has been developed to describe the high-energy limit. It expresses the hadronic scattering of the virtual photon through its fluctuation into a color singlet $q\bar{q}$ pair (or dipole) of a transverse size $r \sim 1/Q$. The dipole is then the hard probe that resolves the small distances inside the proton.

The dipole picture naturally incorporates the description of both inclusive and diffractive events into a common theoretical framework [6,7], as the same dipole scattering amplitudes enter in the formulation of the inclusive and diffractive cross sections. Different saturation parametrizations of the dipole-proton cross section have been successful in describing inclusive and diffractive HERA data. The pioneering work of [8,9] triggered several improvements: the "Dokshitzer-Gribov-Lipatov-Altarelli-Parisi (DGLAP)-improved" model of [10] allows one to include even high-Q^2 data in the fit and the "Balitsky-Kovchegov (BK)-inspired" model of [11] incorporates features from the QCD nonlinear equations.

In diffractive DIS, when the invariant mass M_X of the diffractive final state is much smaller than Q, the dominant contribution to the final state comes from the $q\bar{q}$ component of the photon wave function. By contrast, if $\beta \simeq Q^2/M_X^2 \ll 1$, then the dominant contributions come from the $q\bar{q}g$ component, or from higher Fock states, i.e., from the photon dissociation. The main goal of this work is to improve the description of the $q\bar{q}g$ contribution with respect to previous analysis: it will be modeled in such a way that both the large-Q^2 and small-β limits are implemented.

Including the contributions of heavy quarks in the models has also been a recent concern, as several approaches

*marquet@quark.phy.bnl.gov

observed a decrease of the saturation scale to $Q_s \sim \Lambda_{\mathrm{QCD}}$, when trying to include the charm quark in their analysis [12,13]. This was problematic, however it was recently shown [14] that it is possible to accommodate the model of [11] with heavy-quark contributions and a saturation scale that stays above 1 GeV for $x = 10^{-5}$, rather than dropping to about 500 MeV as is the case in other studies. Our second goal in this paper is to check whether the dipole cross section of this heavy-quark improved saturation model also describes the inclusive diffraction data from HERA.

The plan of the paper is as follows. In Sec. II, we recall the QCD dipole picture for inclusive and diffractive DIS in terms of the dipole-proton scattering. In Sec. III, we discuss in more details the case of diffraction and present the different components of the model, highlighting in each case the improvements with respect to previous approaches, in particular, concerning the inclusion of heavy-quark contributions, and the treatment of impact parameter. Section IV discusses how to implement the $q\bar{q}g$ contribution to the diffractive final state to obtain a unified description that features both the large-Q^2 and small-β limits. In Sec. V, the results of the comparison with the available HERA data are presented, and Sec. VI is devoted to conclusions.

II. QCD DIPOLE PICTURE OF DEEP INELASTIC SCATTERING

We focus on diffractive DIS: $\gamma^* p \to Xp$ (see Fig. 1). With a momentum transfer $t \leq 0$, the proton gets out of the $\gamma^* - p$ collision intact, and there is a rapidity gap between that proton and the final state X whose invariant mass we denote M_X. We recall that the photon virtuality is denoted Q^2, and the $\gamma^* - p$ total energy W. It is convenient to introduce the following variables:

$$x = \frac{Q^2}{Q^2 + W^2}, \qquad \beta = \frac{Q^2}{Q^2 + M_X^2}, \qquad x_{\mathbb{P}} = x/\beta. \quad (1)$$

The $\gamma^* - p$ total cross section $\sigma_{\mathrm{tot}}^{\gamma^* p \to X}$ is usually expressed as a function of x and Q^2, while the diffractive cross section $d\sigma_{\mathrm{diff}}^{\gamma^* p \to Xp}/d\beta dt$ is expressed as a function of β, $x_{\mathbb{P}}$, Q^2, and t. The size of the rapidity gap in the final state is $\ln(1/x_{\mathbb{P}})$.

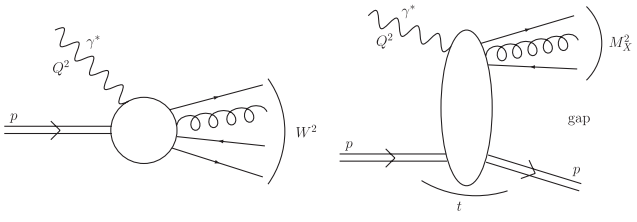

FIG. 1. Representation of $\gamma^* - p$ deep inelastic scattering; inclusive (left) and diffractive (right) events are pictured with the relevant kinematic variables: the photon virtuality Q^2, the energy squared of the $\gamma^* - p$ collision W^2, and in the case of diffraction the momentum transfer t and the invariant mass of the diffractive final state M_X^2.

A. $\gamma^* \to q\bar{q}$ wave functions

To compute those cross sections in the high-energy limit, it is convenient to view the process in a particular frame called the dipole frame. In this frame, the virtual photon undergoes the hadronic interaction via a fluctuation into a colorless $q\bar{q}$ pair, called dipole, which then interacts with the target proton. The wave functions $\psi_\lambda^{f,\alpha\beta}(z, \mathbf{r}; Q^2)$ describing the splitting of a virtual photon with polarization λ into a dipole are well known. The indices α and β denote the spins of the quark and the antiquark composing the dipole of flavor f. The wave functions depend on Q^2, the fraction z of longitudinal momentum (with respect to the $\gamma^* - p$ collision axis) carried by the quark, and the two-dimensional vector $\mathbf{r}$ whose modulus is the transverse size of the dipole.

Formulas giving the functions $\psi_\lambda^{f,\alpha\beta}$ can be found in the literature (see for instance [15]). In what follows, we will need the functions Φ_λ^f which describe the overlap between two wave functions for splitting into dipoles of different transverse size $\mathbf{r}$ and $\mathbf{r}'$:

$$\phi_\lambda^f(z, \mathbf{r}, \mathbf{r}'; Q^2) = N_c \sum_{\alpha\beta} [\psi_\lambda^{f,\alpha\beta}(z, \mathbf{r}'; Q^2)]^* \psi_\lambda^{f,\alpha\beta}(z, \mathbf{r}; Q^2). \quad (2)$$

For a transversely (T) or longitudinally (L) polarized photon, these functions are given by

$$\phi_T^f(z, \mathbf{r}, \mathbf{r}'; Q^2) = \frac{\alpha_{em} N_c}{2\pi^2} e_f^2 \Big((z^2 + (1-z)^2) \varepsilon_f^2 \frac{\mathbf{r}.\mathbf{r}'}{|\mathbf{r}||\mathbf{r}'|} \times K_1(\varepsilon_f |\mathbf{r}|) K_1(\varepsilon_f |\mathbf{r}'|) + m_f^2 K_0(\varepsilon_f |\mathbf{r}|) K_0(\varepsilon_f |\mathbf{r}'|) \Big), \quad (3)$$

$$\phi_L^f(z, \mathbf{r}, \mathbf{r}'; Q^2) = \frac{\alpha_{em} N_c}{2\pi^2} e_f^2 4Q^2 z^2 (1-z)^2 K_0(\varepsilon_f |\mathbf{r}|) \times K_0(\varepsilon_f |\mathbf{r}'|). \quad (4)$$

In the above, e_f and m_f denote the charge and mass of the quark with flavor f and

$$\varepsilon_f^2 = z(1-z)Q^2 + m_f^2. \quad (5)$$

B. Total cross section $\sigma_{\mathrm{tot}}^{\gamma^* p \to X}$

Via the optical theorem, the $\gamma^* - p$ total cross section is related to the elastic scattering of the virtual photon off the proton. In the dipole frame, this happens as follows: at a given impact parameter $\mathbf{b}$, the photon splits into a dipole with a given size $\mathbf{r}$ which scatters elastically off the proton and recombines back into the photon. Therefore the overlap function Φ_λ which enters in the computation of the total cross section is

$$\Phi_\lambda(z, |\mathbf{r}|; Q^2) = \sum_f \phi_\lambda^f(z, \mathbf{r}, \mathbf{r}; Q^2). \tag{6}$$

For a virtual photon with polarization λ, the total cross section is then given by [see Fig. 2(a)]

$$\sigma_\lambda^{\gamma^* p\to X}(x, Q^2) = 2\int d^2r \int_0^1 dz \Phi_\lambda^{\gamma^*\gamma^*}(z, |\mathbf{r}|; Q^2) \times \int d^2b T_{q\bar{q}}(\mathbf{r}, \mathbf{b}; x) \tag{7}$$

where the function $T_{q\bar{q}}(\mathbf{r}, \mathbf{b}; x)$ is the elastic scattering amplitude of the dipole of size $\mathbf{r}$ off the proton at impact parameter $\mathbf{b}$. It contains the x dependence, reflecting the fact that in our frame, the proton carries all the energy and is therefore evolved up to the rapidity $\ln(1/x)$. In the high-energy limit $x \ll 1$ we are considering here, $T_{q\bar{q}}$ does not depend on z.

C. Diffractive cross section $d\sigma_{\mathrm{diff}}^{\gamma^* p\to Xp}/d\beta dt$

The diffractive scattering happens as follows. In the amplitude, the photon splits into a dipole of size $\mathbf{r}$ which scatters off the proton at a given impact parameter $\mathbf{b}$ and dissociates into a final state of invariant mass M_X. The same happens in the complex conjugate amplitude, except that the dipole size $\mathbf{r}'$ and the impact parameter $\mathbf{b}'$ are different from $\mathbf{r}$ and $\mathbf{b}$. Indeed, the final state is characterized by particular values of M_X (or equivalently β) and t, corresponding to particular momenta of the quark and antiquark in the final state. In coordinate space, this imposes two different dipole sizes and impact parameters in the amplitude and the complex conjugate amplitude, therefore the functions $\phi_\lambda^f(z, \mathbf{r}, \mathbf{r}'; Q^2)$ [see (2)] enter in the computation of the diffractive cross section. For a virtual photon with polarization λ, the diffractive cross section is given by [see Fig. 2(b)]

$$\frac{d\sigma_\lambda^{\gamma^* p\to Xp}}{d\beta dt}(\beta, x_{\mathbb{P}}, Q^2, t) = \frac{Q^2}{4\beta^2}\sum_f \int \frac{d^2r}{2\pi}\int \frac{d^2r'}{2\pi}\int_0^1 dz z(1-z)\Theta(\boldsymbol{\kappa}_f^2) e^{i\boldsymbol{\kappa}_f\cdot(\mathbf{r}'-\mathbf{r})}\phi_\lambda^f(z, \mathbf{r}, \mathbf{r}'; Q^2) \times \int d^2b d^2b' e^{i\boldsymbol{\Delta}\cdot(\mathbf{b}'-\mathbf{b})} T_{q\bar{q}}(\mathbf{r}', \mathbf{b}'; x_{\mathbb{P}}). \tag{8}$$

In the above, the differences between $\mathbf{r}$ and $\mathbf{r}'$ on one hand, and $\mathbf{b}$ and $\mathbf{b}'$ on the other hand, are related via Fourier transformation to

$$\boldsymbol{\kappa}_f^2 = z(1-z)Q^2(1-\beta)/\beta - m_f^2 \quad \text{and} \quad \boldsymbol{\Delta}^2 = -t. \tag{9}$$

Note that now the proton is only evolved up to the rapidity $\ln(1/x_{\mathbb{P}})$. This is because some of the energy (M_X^2) is carried by the dipole in order to form the diffractive final state. The dipole is evolved up to a rapidity $\ln(1/\beta)$ and the proton up to the rapidity $\ln(\beta/x) = \ln(1/x_{\mathbb{P}})$. The relevant high-energy limit in this case is $x_{\mathbb{P}} \ll 1$.

Note that to write formula (8), we have neglected possible final states containing gluons. This is justified because these are suppressed by extra powers of α_s. However, if β becomes too small, or if Q^2 becomes too large, the dipole will emit soft or collinear gluons whose emissions are accompanied by large logarithms $\ln(1/\beta)$ or $\ln(Q^2)$ which will compensate the factors of α_s. This will be discussed in more details in Sec. IV, when we explain how to implement the $q\bar{q}g$ contribution to the diffractive final state, in order to correctly describe both the small-β and large-Q^2 limits.

III. SATURATION MODEL FOR THE DIPOLE AMPLITUDE $T_{q\bar{q}}$

Using the dipole picture of deep inelastic scattering, we have expressed the total (7) and diffractive (8) cross sections in the high-energy limit in terms of a single object: the dipole scattering amplitude off the proton $T_{q\bar{q}}(\mathbf{r}, \mathbf{b}; x)$.

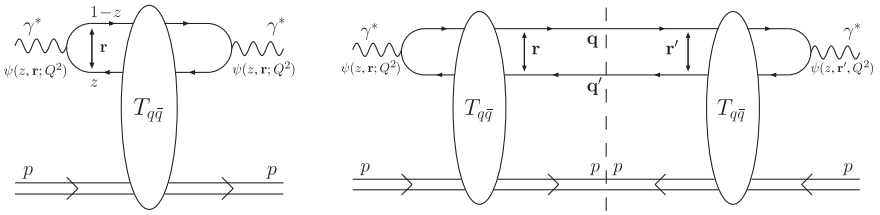

FIG. 2. The QCD dipole picture of deep inelastic scattering. The left diagram represents $\gamma^* - p$ elastic scattering and (via the optical theorem) corresponds to formula (7). The right diagram represents diffractive scattering (without possible final states containing gluons) and corresponds to formula (8). In this case, the final state (indicated by the vertical dashed line) is characterized by $t = -\boldsymbol{\Delta}^2$ and $M_X^2 = (\boldsymbol{\kappa}^2 + m_f^2)/(z(1-z))$, with $\boldsymbol{\Delta} = \mathbf{q} + \mathbf{q}'$ and $\boldsymbol{\kappa} = (1-z)\mathbf{q} - z\mathbf{q}'$ in terms of the quark and antiquark momenta $\mathbf{q}$ and $\mathbf{q}'$. Via Fourier transformations, $\mathbf{q}$ and $\mathbf{q}'$ impose different sizes and impact parameters for the dipole in the amplitude and the dipole in the complex conjugate amplitude.

It is mainly a nonperturbative quantity, but its evolution towards small values of x (or high energy) is computable from perturbative QCD. Evolution equations have been established in the leading $\ln(1/x)$ approximation [16–18] and, at least for central impact parameters, one has learned a lot about the growth of the dipole amplitude and the transition from the leading-twist regime $T_{q\bar{q}} \ll 1$ towards and into the saturation regime $T_{q\bar{q}} \lesssim 1$.

Let us recall that this transition is characterized by the saturation scale $Q_s(x)$, which increases as x decreases. In the following, we shall work in the context of the BK evolution [16] to describe the $\mathbf{r}$ dependence. Indeed, this provides a natural explanation for the geometric scaling properties of the data [3,4]. The impact parameter dependence of $T_{q\bar{q}}$ is still an open problem, it cannot be extracted from perturbative QCD and it is usually modeled. In formulas, one writes

$$T_{q\bar{q}}(\mathbf{r}, \mathbf{b}; x) = S(\mathbf{b}) N(|\mathbf{r}| Q_s(x), x) \tag{10}$$

where we have introduced the factorized impact-parameter profile $S(\mathbf{b})$. In the following, we detail the different components of our model: $S(\mathbf{b})$ and $N(|\mathbf{r}|Q_s, x)$.

A. Impact-parameter profile $S(\mathbf{b})$

When performing the $\mathbf{b}$ integration in formula (7), this contributes only to the normalization via a constant factor $2\int d^2b S(\mathbf{b}) = \sigma_0$ (of order 25 mb) characterizing the transverse area of the proton. However, in the case of the diffractive cross section (8), the $\mathbf{b}$ integration gives the momentum transfer dependence. Experimentally, the diffractive cross section decreases exponentially with $|t|$ as $e^{B_D t}$, where B_D is the diffractive slope (of order 6 GeV^{-2}). This is consistent with the Gaussian profile $S(\mathbf{b}) = e^{-\mathbf{b}^2/(2B_D)}$, which then implies $\sigma_0 = 4\pi B_D$.

In the literature, the quantities σ_0 and B_D are usually considered unrelated, however as we have shown, a consistent treatment of the impact parameter dependence within the dipole picture implies that this is not the case. To summarize, one has

$$\frac{d\sigma}{dt} \sim e^{B_D t} \Rightarrow S(\mathbf{b}) = e^{-\mathbf{b}^2/(2B_D)} \Rightarrow \sigma_0 = 4\pi B_D. \tag{11}$$

B. Heavy-quark improved Iancu-Itakura-Munier (IIM) saturation model for $N(|\mathbf{r}|Q_s, x)$

The Iancu-Itakura-Munier (IIM) saturation model is inspired by universal properties [19] of solutions of the BK equation [16]. The most important feature is probably the geometric scaling regime: at small values of x, instead of being a function of *a priori* the two variables $r = |\mathbf{r}|$ and x, N is actually a function of the single variable $rQ_s(x)$ up to inverse dipole sizes significantly larger than the saturation scale $Q_s(x)$. If $rQ_s > 1$ then $N = 1$ and the scaling is obvious. We insist that the scaling property is a nontrivial prediction for $rQ_s \ll 1$, when N is still much smaller than 1.

Of course the geometric scaling window has a limited extension: at very small dipole sizes, deep into the leading-twist regime, the scaling breaks down. Universal scaling violations [19] due to x not being small enough have also been derived and are implemented in the IIM model, which is therefore a function of rQ_s and x. Recently, a new type of geometric scaling violations has been predicted, due to the inclusion of Pomeron loops in the evolution [18,20] (the BK equation only resums fan diagrams). These violations transform the geometric scaling regime into an intermediate energy regime, as they arise at very small values of x in the so-called diffusive scaling regime. This new regime is likely out of the reach of HERA and we shall not address it in this study.

In the IIM model, the saturation scale is parametrized by

$$Q_s(x) = \left(\frac{x_0}{x}\right)^{\lambda/2} \text{GeV} \tag{12}$$

and the dipole amplitude is given by

$$N(rQ_s, x) = \begin{cases} N_0 \left(\frac{rQ_s}{2}\right)^{2\gamma_c} \exp\left[-\frac{2\ln^2(rQ_s/2)}{\kappa\lambda\ln(1/x)}\right] & \text{for } rQ_s \le 2 \\ 1 - e^{-4\alpha\ln^2(\beta rQ_s)} & \text{for } rQ_s > 2 \end{cases} \tag{13}$$

with α and β uniquely determined from the conditions that N and its derivative are continuous at $rQ_s = 2$. The amplitude at the matching point is chosen to be $N_0 = 0.7$.

In this work, we shall consider the IIM saturation model [11] extended in [14] to include heavy quarks (with $m_c = 1.4$ GeV, $m_b = 4.5$ GeV, and $m_f = 0.14$ GeV for the light flavors). The coefficient $\kappa = 9.9$ is obtained from the Balitsky-Fadin-Kuraev-Lipatov (BFKL) kernel while the critical exponent $\gamma_c = 0.7376$ is fitted to the HERA measurements of the proton structure function, along with the remaining parameters. The saturation scale parameters are $\lambda = 0.2197$ and $x_0 = 1.632 \times 10^{-5}$ and the cross section at saturation is $\sigma_0 = 70.26$ GeV^{-2} (or 27.36 mb). Note that, via $\sigma_0 = 4\pi B_D$, this corresponds to the diffractive slope $B_D = 5.591$ GeV^{-2}, which is in agreement with the experimental observations [21,22].

C. $q\bar{q}$ components of the diffractive structure functions

Let us introduce the transverse and longitudinal diffractive structure functions $F_T^{D,3}(\beta, x_{\mathbb{P}}, Q^2)$ and $F_L^{D,3}(\beta, x_{\mathbb{P}}, Q^2)$. They are easily obtained from the diffractive cross sections $d\sigma_\lambda^{\gamma^* p \to X p}/d\beta$, integrated over the momentum transfer t. In practice, one does not actually carry out the t integration of (8), but one rather uses the fact that the diffractive cross section decreases exponentially with $|t|$ like $e^{B_D t}$. One writes:

$$x_{\mathbb{P}}F_{\lambda}^{D,3} = \frac{Q^2\beta}{4\pi^2\alpha_{em}}\frac{d\sigma_{\lambda}^{\gamma^* p\to Xp}}{d\beta},$$
$$\frac{d\sigma_{\lambda}^{\gamma^* p\to Xp}}{d\beta} = \int_{t_{\min}}^{0} dt \frac{d\sigma_{\lambda}^{\gamma^* p\to Xp}}{d\beta dt} \simeq \frac{1}{B_D}\frac{d\sigma_{\lambda}^{\gamma^* p\to Xp}}{d\beta dt}\Big|_{t=0}, \quad (14)$$

with $e^{B_D t_{\min}} \ll 1$ (in practice, $t_{\min} = -1\ \mathrm{GeV}^2$). When computing (8) for $t = 0$, the two impact parameter integrations yield the factor $\sigma_0^2/4$. As already discussed, a consistent treatment of the impact parameter dependence of the dipole scattering amplitude $T_{q\bar{q}}$ implies $\sigma_0^2/(4B_D) = \pi\sigma_0$, which we shall use in what follows.

Note that one could also study $F_T^{D,4}$ and $F_L^{D,4}$ directly. However, there is less data for those t-dependent structure functions, and they would not further test our model, which has the exponential decrease $e^{B_D t}$ built in. This type of measurement would rather be interesting to test saturation models which feature a t-dependent saturation scale, as predicted in [23] from the full BK equation.

Let us come back to the diffractive structure functions $F_{\lambda}^{D,3}$. From formulas (8), (10), and (14), one obtains the contributions from the $q\bar{q}$ final state. Using the transverse overlap function (3), one gets

$$x_{\mathbb{P}}F_T^{q\bar{q}}(\beta, x_{\mathbb{P}}, Q^2) = \frac{\sigma_0 N_c}{32\pi^3}\frac{Q^4}{\beta}\sum_f e_f^2 \int_0^1 dz\Theta(\kappa_f^2) z(1-z) \times [(z^2+(1-z)^2)(z(1-z)Q^2 + m_f^2) I_1^2(\kappa_f, \epsilon_f, Q_s) + m_f^2 I_0^2(\kappa_f, \epsilon_f, Q_s)] \quad (15)$$

for the $q\bar{q}$ contribution to the transverse diffractive structure function. With the longitudinal overlap function (4), one gets the $q\bar{q}$ contribution to the longitudinal diffractive structure function:

$$x_{\mathbb{P}}F_L^{q\bar{q}}(\beta, x_{\mathbb{P}}, Q^2) = \frac{\sigma_0 N_c}{32\pi^3}\frac{Q^4}{\beta}\sum_f e_f^2 \int_0^1 dz\Theta(\kappa_f^2) \times 4Q^2 z^3(1-z)^3 I_0^2(\kappa_f, \epsilon_f, Q_s). \quad (16)$$

In (15) and (16), the functions I_λ are given by

$$I_\lambda(\kappa, \epsilon, Q_s) = \int_0^\infty r dr J_\lambda(\kappa r) K_\lambda(\epsilon r) N(rQ_s, x_{\mathbb{P}}) \quad (17)$$

in terms of the dipole scattering amplitude $N(rQ_s, x_{\mathbb{P}})$ and of the Bessel functions J_λ and K_λ.

IV. $q\bar{q}g$ CONTRIBUTION TO THE DIFFRACTIVE FINAL STATE

As pictured in Fig. 2, formula (8) is the contribution of the $q\bar{q}$ final state to the diffractive cross section. We have neglected possible final states containing gluons, and in general it is justified because these are suppressed by extra powers of α_s. However, there are two kinematical regimes for which this is not the case: the large-Q^2 limit and the small-β limit. In those situations, gluon emissions are accompanied by large logarithms $\ln(Q^2)$ or $\ln(1/\beta)$ which compensate the factors of α_s, and multiple gluons emissions should be resummed to complete formula (8).

In practice, including the $q\bar{q}g$ final state is enough to describe the HERA data, and this can be done within the dipole picture in both limits, at leading $\ln(Q^2)$ [9,24] or leading $\ln(1/\beta)$ accuracy [25–29], as we recall in this section. Note that, at leading $\ln(1/\beta)$ accuracy, all multiple soft gluon emissions can also be accounted for in the dipole picture [20,30], but we shall restrict this phenomenological study to the $q\bar{q}g$ contribution.

The most popular approach is to consider the large-Q^2 limit to implement the $q\bar{q}g$ contribution [9,12,31], even though the experimental measurements do not reach very high values of Q^2. In fact, the contribution of the $q\bar{q}g$ final state is important only for small values of β which, due to the finite energy available, correspond to rather small values of Q^2. This is not satisfactory. In this paper, the $q\bar{q}g$ contribution to the diffractive final state is modeled in such a way that both the large-Q^2 and small-β limits are implemented.

A. Large-Q^2 limit

At large Q^2, the contribution of the $X = q\bar{q}g$ final state in diffractive $\gamma^* p \to Xp$ scattering was computed in [24,32]. In momentum space, the collinear gluon has a transverse momentum much smaller than Q^2. In coordinate space, the scattering involves a gluonic gg dipole [see Fig. 3(a)]: the transverse distance between the quark and the antiquark is much smaller than the transverse distance between the quark and the gluon. The $q\bar{q}$ pair on one side and the gluon on the other side form an effective gluonic color dipole which undergoes the hadronic interaction [24]. We shall denote the corresponding scattering amplitude off the proton $T_{gg}(\mathbf{r}, \mathbf{b}; x)$ for a dipole of size $\mathbf{r}$ at impact parameter $\mathbf{b}$. With our model for impact parameter dependence, we write

$$T_{gg}(\mathbf{r}, \mathbf{b}; x_{\mathbb{P}}) = S(\mathbf{b})\tilde{N}(|\mathbf{r}|Q_s(x), x_{\mathbb{P}}) \quad (18)$$

where $\tilde{N}$ is the equivalent of N but for a gg dipole.

At leading $\ln(Q^2)$, the $q\bar{q}g$ final state contributes only to the transverse diffractive structure function and one has

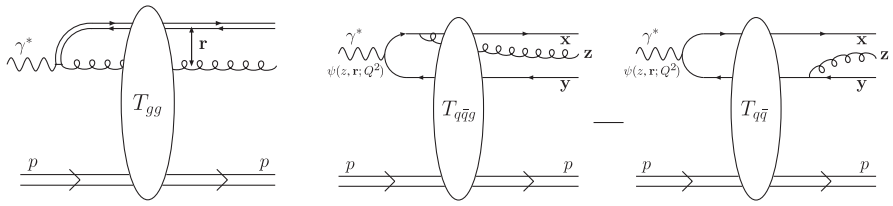

FIG. 3. The contribution of the $X = q\bar{q}g$ final state in diffractive $\gamma^* p \to Xp$ scattering. Left diagram: at large Q^2; the quark-antiquark transverse distance is much smaller than the quark-gluon transverse distance and an effective gg dipole scatters off the proton. Right diagram: at small β; the quark-antiquark-gluon triplet scatters after the gluon emission and the quark-antiquark pair scatters before the gluon emission, with a relative minus sign. In both cases only the amplitude is shown, it has to be squared to obtain the cross section.

$$x_{\mathbb{P}} F_T^{q\bar{q}g}|_{LL(Q^2)}(\beta, x_{\mathbb{P}}, Q^2) = \frac{\sigma_0 \alpha_s C_F N_c \beta}{32\pi^4} \sum_f e_f^2 \int_0^{Q^2} dk^2 \ln\left(\frac{Q^2}{k^2}\right) \int_\beta^1 dz \left[\left(1-\frac{\beta}{z}\right)^2 + \left(\frac{\beta}{z}\right)^2\right] I_g^2(\sqrt{1-z}, \sqrt{z}, Q_s/k) \quad (19)$$

with

$$I_g(a, b, c) = \int_0^\infty r dr J_2(ar) K_2(br) \tilde{N}(cr, x_{\mathbb{P}}). \quad (20)$$

The computation of [24] is a leading-twist two-gluon exchange calculation in which the gg dipole is given by $\tilde{N}(rQ_s, x) = N_c N(rQ_s, x)/C_F$ in terms of the $q\bar{q}$ dipole. However this is not consistent with the use of a saturation model. For instance, $\tilde{N}$ should saturate at 1, not at N_c/C_F. This implies that, when using (19) and (20) with $\tilde{N} = N_c N/C_F$ and a saturation model for N, the analysis in the literature overestimate the $q\bar{q}g$ contribution. In practice, this is usually compensated by using an unphysically small value for α_s.

The parametrization we shall use in this paper is $\tilde{N} = 2N - N^2$. This relation implies the large-N_c limit, and therefore goes well with our model for the $q\bar{q}$ dipole scattering amplitude N: it is consistent with the BK evolution implemented in (13). Numerically, this reduces the $q\bar{q}g$ contribution (with respect to using $\tilde{N} = N_c N/C_F$), especially because the saturation scale is quite large, and therefore N is not always small.

Finally, when computing the heavy quark contributions $c\bar{c}g$ and $b\bar{b}g$, we replace the β variable in (19) by $\beta(1 + 4m_f^2/Q^2)$. This substitution, which modifies only the small-Q^2 results, is necessary in order to insure that there is no $q\bar{q}g$ contributions when the final state is such that $M_X = 2m_f$ (in practice, such a substitution does not make a difference for the light quarks).

B. Small-β limit

At small β, the contribution of the $X = q\bar{q}g$ final state in diffractive $\gamma^* p \to Xp$ scattering was computed in many studies [25–29]. In coordinate space, denoting $\mathbf{x}$ the transverse position of the quark, $\mathbf{y}$ that of the antiquark, and $\mathbf{z}$ that of the gluon, the diffractive scattering is expressed in terms of [see Fig. 3(b)]

$$[T_{q\bar{q}g}(\mathbf{x}, \mathbf{y}, \mathbf{z}; x_{\mathbb{P}}) - T_{q\bar{q}}(\mathbf{x}, \mathbf{y}; x_{\mathbb{P}})]^2 = S^2(\mathbf{b})[N^{(2)}(|\mathbf{r}'|Q_s, |\mathbf{r} - \mathbf{r}'|Q_s, x_{\mathbb{P}}) - N(|\mathbf{r}|Q_s, x_{\mathbb{P}})]^2. \quad (21)$$

In the left-hand side, the virtual contribution $T_{q\bar{q}}$ represents the scattering of the quark-antiquark pair, before the gluon emission. Within our model for the impact parameter $\mathbf{b} = (\mathbf{x} + \mathbf{y})/2$, one has $T_{q\bar{q}}(\mathbf{x}, \mathbf{y}; x_{\mathbb{P}}) = S(\mathbf{b}) N(|\mathbf{r}|Q_s, x_{\mathbb{P}})$ where the dipole size is naturally $\mathbf{r} = \mathbf{x} - \mathbf{y}$. The real contribution $T_{q\bar{q}g}$ represents the scattering of the quark-antiquark-gluon triplet, after the gluon emission. In the right-hand side, we factorized the impact-parameter profile and wrote $T_{q\bar{q}g}(\mathbf{x}, \mathbf{y}, \mathbf{z}; x_{\mathbb{P}}) = S(\mathbf{b}) N^{(2)}(|\mathbf{r}'|Q_s, |\mathbf{r} - \mathbf{r}'|Q_s, x_{\mathbb{P}})$ with $\mathbf{r}' = \mathbf{x} - \mathbf{z}$ (and $\mathbf{r} - \mathbf{r}' = \mathbf{z} - \mathbf{y}$).

In the context of the BK evolution implemented in (13), the link between $N^{(2)}$ and N comes from the fact that the scattering of the $q\bar{q}g$ triplet is equivalent to the scattering of two dipoles with sizes $\mathbf{r}'$ and $\mathbf{r} - \mathbf{r}'$ (a dipole emitting a soft gluon is equivalent to a dipole splitting into two dipoles). Therefore our model for $N^{(2)}$ is

$$N^{(2)}(|\mathbf{r}'|Q_s, |\mathbf{r} - \mathbf{r}'|Q_s, x_{\mathbb{P}}) = N(|\mathbf{r}'|Q_s, x_{\mathbb{P}}) + N(|\mathbf{r} - \mathbf{r}'|Q_s, x_{\mathbb{P}}) - N(|\mathbf{r}'|Q_s, x_{\mathbb{P}}) N(|\mathbf{r} - \mathbf{r}'|Q_s, x_{\mathbb{P}}). \quad (22)$$

At leading $\ln(1/\beta)$, the contribution of the $q\bar{q}g$ final state to the transverse diffractive structure function is

$$x_{\mathbb{P}} F_T^{q\bar{q}g}|_{LL(1/\beta)}(x_{\mathbb{P}}, Q^2) = \frac{C_F \alpha_s Q^2 \sigma_0}{8\pi^3 \alpha_{em}} \int_0^\infty r dr \times \int_0^1 dz \Phi_T(z, r; Q^2) A(r, x_{\mathbb{P}}) \quad (23)$$

with

$$A(|\mathbf{r}|, x_{\mathbb{P}}) = \int d^2r' \frac{\mathbf{r}^2}{\mathbf{r}'^2(\mathbf{r}-\mathbf{r}')^2}[N(|\mathbf{r}'|Q_s, x_{\mathbb{P}}) + N(|\mathbf{r}-\mathbf{r}'|Q_s, x_{\mathbb{P}}) - N(|\mathbf{r}|Q_s, x_{\mathbb{P}}) - N(|\mathbf{r}'|Q_s, x_{\mathbb{P}})N(|\mathbf{r}-\mathbf{r}'|Q_s, x_{\mathbb{P}})]^2. \quad (24)$$

It is independent of β because the structure function $F^{D,3} \sim \beta d\sigma^{\gamma^* p \to Xp}/d\beta$ picks up the coefficient of $\ln(1/\beta)$ in $\sigma^{\gamma^* p \to Xp}$. Also, the overlap function is Φ_T because in the leading $\ln(1/\beta)$ approximation, the final state mass M_X is fixed only by the soft gluon longitudinal momentum, and therefore transverse sizes are the same in the amplitude and the complex conjugate amplitude.

Note that in (23), the impact parameter integration $\int d^2b S^2(\mathbf{b})$ yielded a factor $\sigma_0/4$. If the $\mathbf{b}$ profile was a theta function as assumed in [28], the $q\bar{q}g$ contribution would be a factor of 2 higher. In what follows, to numerically compute $A(r, x_{\mathbb{P}})$, we use the clever change of variables introduced in [28] that we recall in Appendix A.

C. Model for $x_{\mathbb{P}}F_T^{q\bar{q}g}$

The usual approach to implement the $q\bar{q}g$ contribution is to use formula (19), but as we shall see, this is not correct for small values of β. Let us consider the $q\bar{q}g$ contribution for $\beta = 0$. By definition, the correct result is $F_T^{q\bar{q}g}|_{\ln(1/\beta)}$ given in formulas (23) and (24). By contrast, the small-β limit of the leading $\ln(Q^2)$ contribution $F_T^{q\bar{q}g}|_{LL(Q^2)}$ is

$$x_{\mathbb{P}}F_T^{q\bar{q}g}|_{LL(Q^2)}(\beta=0, x_{\mathbb{P}}, Q^2) = \frac{C_F N_c \alpha_s \sigma_0}{12\pi^4}\sum_f e_f^2 \int_0^{Q^2} dk^2 \left[\ln\left(\frac{Q^2}{k^2}\right)\right] \left| \int_0^\infty \frac{dr}{r} J_2(kr)(2N(rQ_s, x_{\mathbb{P}}) - N^2(rQ_s, x_{\mathbb{P}}))\right|^2 \quad (25)$$

where we have used (19) with $K_2(x) = 2/x^2$ for $x \to 0$. Formula (25) shows that, after rising as β decreases, the diffractive structure function goes to a constant. This constant is different from the correct result (23) and (24), except for very large values of Q^2, for which $F_T^{q\bar{q}g}|_{LL(Q^2)}$ is correct by definition. And indeed, if $Q^2 \gg Q_s^2$, the two formulas coincide to give

$$x_{\mathbb{P}}F_T^{q\bar{q}g}(\beta=0, x_{\mathbb{P}}, Q^2 \gg Q_s^2) = \frac{C_F N_c \alpha_s Q_s^2 \sigma_0}{6\pi^4}\sum_f e_f^2 \ln\left(\frac{Q^2}{Q_s^2}\right)\int_0^\infty \frac{d\bar{r}}{\bar{r}^3}[2N(\bar{r}, x_{\mathbb{P}}) - N^2(\bar{r}, x_{\mathbb{P}})]^2. \quad (26)$$

This is shown analytically in Appendix B. In Fig. 4, we compare formulas (23)–(25) as a function of Q^2 and for different value of $x_{\mathbb{P}}$. One sees that when Q^2 increases, the ratio between the two results gets closer to one, but that limit is only reached for very large values of Q^2 not shown in the figure. For the values of Q^2 in the HERA range, the actual result is smaller than the leading $\ln(Q^2)$ one by a factor of about 0.6.

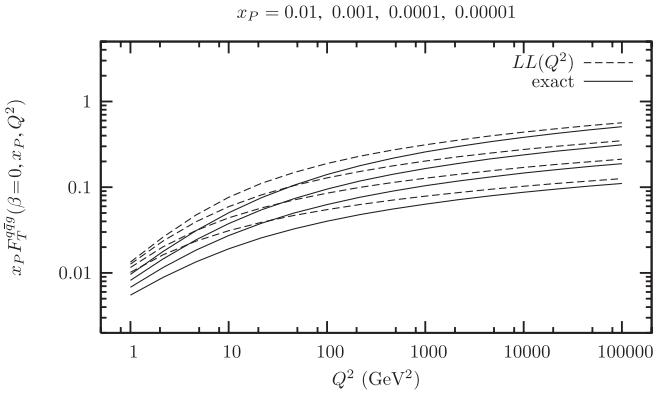

FIG. 4. The contribution of the $q\bar{q}g$ final state to the transverse diffractive structure function $F_T^{q\bar{q}g}$ at $\beta = 0$ as a function of Q^2. The full lines show the exact result $F_T^{q\bar{q}g}|_{LL(1/\beta)}$ while the dashed lines show the leading $\ln(Q^2)$ result $F_T^{q\bar{q}g}|_{LL(Q^2)}$. Different sets of curves are for different values of $x_{\mathbb{P}} = 0.01, 0.001, 0.0001, 0.000\,01$, from bottom to top. As Q^2 increases the two results get closer, but they coincide for only very large values of Q^2.

In order to have the correct $q\bar{q}g$ contribution for small values of β, we shall use the following model:

$$x_{\mathbb{P}}F_T^{q\bar{q}g}(\beta, x_{\mathbb{P}}, Q^2) = x_{\mathbb{P}}F_T^{q\bar{q}g}|_{LL(Q^2)}(\beta, x_{\mathbb{P}}, Q^2) \times \frac{F_T^{q\bar{q}g}|_{LL(1/\beta)}(x_{\mathbb{P}}, Q^2)}{F_T^{q\bar{q}g}|_{LL(Q^2)}(\beta=0, x_{\mathbb{P}}, Q^2)} \quad (27)$$

obtained from formulas (19), (20), and (23)–(25). It is such that $F_T^{q\bar{q}g} = F_T^{q\bar{q}g}|_{LL(Q^2)}$ at large Q^2 and $F_T^{q\bar{q}g} = F_T^{q\bar{q}g}|_{LL(1/\beta)}$ at small β. In the small-Q^2 and large-β region, the $q\bar{q}g$ contribution may not be correctly described. However in this case, the diffractive structure function is dominated by the $q\bar{q}$ component, and the $q\bar{q}g$ contribution is not relevant.

Finally we point out that our implementation of the $q\bar{q}g$ contribution is parameter free, the only uncertainty being related to the value of α_s. The average value of Q^2 in diffractive measurements at HERA is about 10 GeV^2, therefore we choose $\alpha_s = 0.25$, which corresponds to such a scale.

V. DESCRIPTION OF THE HERA DATA

The H1 and ZEUS experiments at HERA have measured the diffractive cross section for the process $ep \to eXp$,

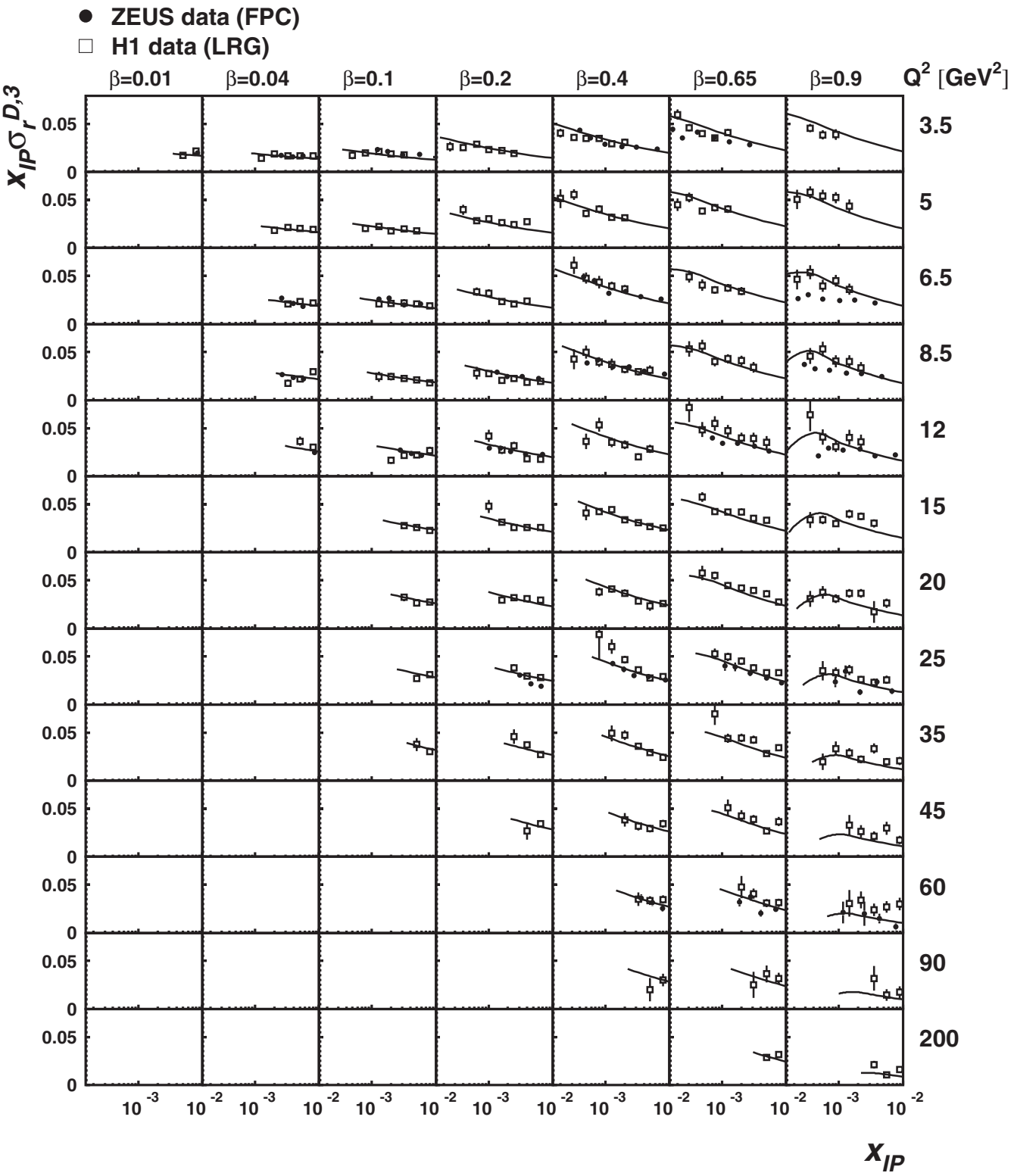

FIG. 5. $x_{\mathbb{P}}\sigma_r^{D,3}(\beta, x_{\mathbb{P}}, Q^2)$ as a function of $x_{\mathbb{P}}$ for different values of β and Q^2. The H1 (LRG) and ZEUS (FPC) diffractive data are compared to the predictions of our model, and the $x_{\mathbb{P}}$ range is restricted to $x_{\mathbb{P}} < 0.01$. In this figure, the H1 data are unchanged and it is our predictions which are multiplied by the factor 1.23. The ZEUS data are multiplied by 0.85 in order to convert them to the H1 M_Y range and the bin centers have been shifted to the H1 values using a parametrization given in [34]. Only the statistical part of the uncertainty is shown for the data points on this plot. The shape of the curves in the $\beta = 0.9$ bins is due to the fact that the contribution of $F_L^{D,3}$ to the reduced cross section is important for large values of β.

tagging the proton in the final state. After integrating the squared momentum transfer dependence from $t_{\min} = -1$ GeV^2 to $t = 0$, the data are presented in terms of the reduced cross section $\sigma_r^{D,3}(\beta, x_{\mathbb{P}}, Q^2)$:

$$\frac{d^3\sigma^{ep\to eXp}}{dx_{\mathbb{P}}d\beta dQ^2} = \frac{4\pi\alpha_{em}^2}{\beta Q^4}\left(1 - y + \frac{y^2}{2}\right)\sigma_r^{D,3}(\beta, x_{\mathbb{P}}, Q^2),$$
$$\sigma_r^{D,3} = F_T^{D,3} + \frac{2-2y}{2-2y+y^2}F_L^{D,3}. \quad (28)$$

with $y = Q^2/(sx)$ where $\sqrt{s} = 318$ GeV is the total energy in the $e - p$ collision. We shall call the corresponding data sets the LPS [21] (ZEUS) and FPS [22] (H1) data.

The H1 and ZEUS experiments have also measured the diffractive cross section for the process $ep \to eXY$, selecting events with a large rapidity gap between the systems X and Y in case of H1 [33], and using the so-called M_X method in case of ZEUS [34]. Y represents the scattered proton, either intact or in a low-mass excited state, with $M_Y < 1.6$ GeV (H1) or $M_Y < 2.3$ GeV (ZEUS). The cut on the squared momentum transfer t at the proton vertex is again $t > -1$ GeV^2 for both experiments. We shall call the corresponding data sets the FPC [34] (ZEUS) and LRG [33] (H1) data.

Because they include events in which the proton has broken up, the cross sections measured for the process $ep \to eXY$ are larger than the one measured for the process $ep \to eXp$. Also, because H1 and ZEUS measurements are performed with different M_Y cuts, the ZEUS cross section is bigger than the H1 cross section, for which the proton-dissociative events are more reduced. However, within the kinematical ranges of the measurements, it seems that the differences are constant factors: the FPC and LRG data points can be converted to the FPS-LPS ones by dividing the cross sections by 1.45 and 1.23 respectively [33,34]. Note that it is the FPS-LPS data that correspond to our definition of diffractive events and to our formulas, as the proton should truly escape the collision intact.

In our model, the reduced cross section $\sigma_r^{D,3}(\beta, x_{\mathbb{P}}, Q^2)$ is given in terms of the diffractive structure functions by

$$x_{\mathbb{P}}\sigma_r^{D,3} = x_{\mathbb{P}}F_T^{q\bar{q}} + x_{\mathbb{P}}F_T^{q\bar{q}g} + \frac{2-2y}{2-2y+y^2}x_{\mathbb{P}}F_L^{q\bar{q}}. \quad (29)$$

Using formulas (15), (16), and (27), and the dipole scattering amplitude (13), we obtain a parameter-free calculation for $x_{\mathbb{P}}\sigma_r^{D,3}$ that we can compare to the data. Diffractive DIS measurements are sensitive to the saturation regime of QCD only for small values of $x_{\mathbb{P}}$, therefore we shall only consider experimental data which feature $x_{\mathbb{P}} < 10^{-2}$ in our comparisons. Note that we do not include any $q\bar{q}g$ contribution to the longitudinal structure function: for small values of β it could be sizeable, but for kinematical reasons small β is associated with y close to 1, in which case $F_L^{D,3}$ does not contribute to $\sigma_r^{D,3}$.

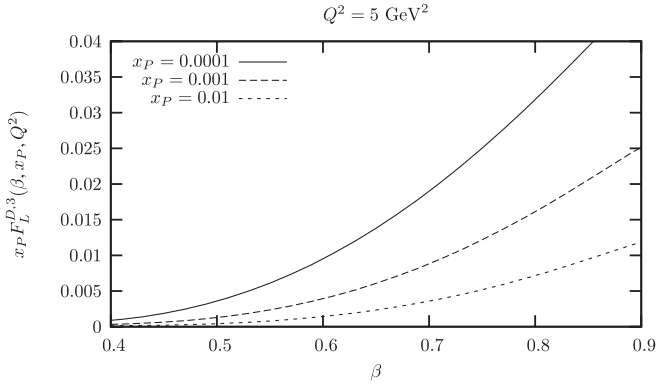

FIG. 6. Predictions for the longitudinal diffractive structure function. $x_{\mathbb{P}}F_L^{D,3}(\beta, x_{\mathbb{P}}, Q^2)$ is plotted as a function of β for $Q^2 = 5$ GeV^2 and for different values of $x_{\mathbb{P}} = 0.01, 0.001, 0.0001$. With our parametrization, only the $q\bar{q}$ final state contributes.

To estimate the quality of our description, we performed the following χ^2 computations, adding statistical and systematic uncertainties in quadrature. Within the LPS + FPS ($ep \to eXp$) data sets, 76 points pass the $x_{\mathbb{P}} < 0.01$ cut and we obtain $\chi^2/\text{points} = 0.80$. When comparing to the 4 data sets, with the proper renormalizations for the FPC and LRG ($ep \to eXY$) measurements, 343 points pass the $x_{\mathbb{P}} < 0.01$ cut and we obtain $\chi^2/\text{points} = 1.28$. This is a quite good description, considering our predictions are parameter free. As an illustration, Fig. 5 displays a comparison of our predictions with the FPC + LRG data. We also checked the agreement with the charm contribution to $\sigma_r^{D,3}$ using the few points available [35], one obtains $\chi^2/\text{points} = 0.68$.

Note that, if the running coupling $\alpha_s(Q^2)$ is used in the $q\bar{q}g$ contribution (instead of imposing $\alpha_s = 0.25$), the description of $\sigma_r^{D,3}$ is also very good with similar values of χ^2/points: 0.63 when comparing to the LPS and FPS data, and 1.20 when comparing to the four data sets. In this case, the additional cut $Q^2 > 1$ GeV^2 is used in order to keep the coupling reasonably small (this only removes 15 of the LPS points). We also noticed that it is possible to obtain a description of equal quality without the correction $F_T^{q\bar{q}g}|_{LL(1/\beta)}/F_T^{q\bar{q}g}|_{LL(Q^2)}$ in the $q\bar{q}g$ contribution (27), if one imposes an unphysically small value for the coupling: $\alpha_s = 0.15$.

Finally, Fig. 6 shows predictions for the longitudinal diffractive structure function $F_L^{D,3}(\beta, x_{\mathbb{P}}, Q^2)$, which in our approach is obtained from the $q\bar{q}$ contribution $F_L^{q\bar{q}}$ [see formula (16)].

VI. CONCLUSIONS

We presented a new description of HERA diffractive deep inelastic scattering data. It uses the parametrization for the dipole scattering amplitude obtained in [14]. This is an extension of the IIM saturation model which contains

heavy-quark contributions. Contrary to previous studies, it features a saturation scale $Q_s(x)$ that stays above 1 GeV for $x = 10^{-5}$, rather than dropping by a factor of 2 after including heavy-quark contributions. Our description of the data is parameter-free and, in the regime $x_{\mathbb{P}} < 0.01$, it features values of χ^2/points of order 1.

Let us recall the improvements that our model brings with respect to previous approaches.

(i) Instead of considering the dipole cross section σ_0 and the diffractive slope B_D as independent quantities, we use the relation (11). It results from a consistent treatment of the impact parameter dependence of the dipole scattering amplitude. Compared to previous approaches, it removes the possibility to adjust B_D.

(ii) In the large-Q^2 limit, the $q\bar{q}g$ contribution to the diffractive final state is described by a gg dipole. By contrast with previous approaches, it is expressed in terms of the $q\bar{q}$ dipole in such a way that it is consistent with unitarity ($\tilde{N} \leq 1$), yielding a more satisfactory description.

(iii) The $q\bar{q}g$ contribution to the diffractive final state is modeled in such a way that both the large-Q^2 and small-β limits are implemented (27). For the values of Q^2 in the HERA range, the resulting $q\bar{q}g$ contribution is smaller than the leading $\ln(Q^2)$ result used in previous descriptions. This allows one to have a good description of the data with a value of α_s (either fixed at $\alpha_s = 0.25$ or running with Q^2) that is not unphysically small.

(iv) Our predictions include correctly the contribution of the longitudinal diffractive structure function $F_L^{D,3}$: we predict $\sigma_r^{D,3}$, not $F_2^{D,3} = F_T^{D,3} + F_L^{D,3}$.

(v) When comparing our predictions to the experimental data, the comparison is made with the $ep \to eXp$ data unchanged and the $ep \to eXY$ data renormalized, and not the opposite. Our definition of diffractive events (and our formulas) is such that the proton truly escapes the collision intact.

Of all the possible descriptions of diffractive DIS data (for a global analysis, see [36]), the dipole picture is the one which is adapted to study the physics of parton saturation. Having a consistent saturation model to describe hard diffraction in $e - p$ scattering represent a good foundation for further works. On the phenomenological side, studying hard diffraction in $e - A$ becomes of interest [37], as it is an ideal process to investigate the saturation regime of QCD that could be explored at a future electron-ion collider. On the theoretical side, many new developments improved our understanding of the QCD nonlinear evolution, and their consequences are to be investigated [20,38].

ACKNOWLEDGMENTS

I am grateful to Grégory Soyez for sharing his results [14] on the heavy-quark improved IIM saturation model while they were still preliminary. I am also grateful to Laurent Schoeffel for helping collect the HERA data on inclusive diffraction, for helping building up Fig. 5, and for useful clarifications concerning the experimental measurements. I would like to thank them as well as Tuomas Lappi and Raju Venugopalan for insightful discussions concerning several aspects of this work. I also acknowledge Krzyzstof Golec-Biernat and Robi Peschanski for useful suggestions. I thank the Galileo Galilei Institute for Theoretical Physics for hospitality and the INFN for partial support during the completion of part of this work. This research was supported in part by RIKEN, Brookhaven National Laboratory and the U.S. Department of Energy (DE-AC02-98CH10886).

APPENDIX A: NUMERICAL COMPUTATION OF $A(|\mathbf{r}|, x_{\mathbb{P}})$

In this Appendix, following [28], we show how to transform the expression [see formula (24)]

$$A(|\mathbf{r}|, x_{\mathbb{P}}) = \int d^2r' \frac{\mathbf{r}^2}{\mathbf{r}'^2(\mathbf{r}-\mathbf{r}')^2}[N(|\mathbf{r}'|Q_s, x_{\mathbb{P}}) + N(|\mathbf{r}-\mathbf{r}'|Q_s, x_{\mathbb{P}}) - N(|\mathbf{r}|Q_s, x_{\mathbb{P}}) - N(|\mathbf{r}'|Q_s, x_{\mathbb{P}})N(|\mathbf{r}-\mathbf{r}'|Q_s, x_{\mathbb{P}})]^2 \quad \text{(A1)}$$

in order to estimate it numerically. Writing the two-dimensional integration in the complex plane and introducing $S = 1 - N$, we obtain (with $r = |\mathbf{r}|$)

$$A(r, x_{\mathbb{P}}) = \int \frac{dzd\bar{z}}{2|z|^2|1-z|^2}[S(|z|rQ_s, x_{\mathbb{P}})S(|1-z|rQ_s, x_{\mathbb{P}}) - S(rQ_s, x_{\mathbb{P}})]^2. \quad \text{(A2)}$$

We then follow the following procedure.

(i) $|z|$ and $|1-z|$ are invariant by symmetry with respect to the real axis so one can multiply the integral by 2 and restrict ourselves to the upper part of the complex plane.

(ii) For $|z| \leq 1$, let us change the variables into $u = |z| \in [0,1]$ and $v = \frac{|1-z|+|z|-1}{2|z|} \in [0,1]$, this implies

$$dzd\bar{z} = \frac{8|z|^2|1-z|dudv}{|z-\bar{z}|} \qquad |1-z||z-\bar{z}| = 4u(1-u+2uv)\sqrt{v(1-v)(1+uv)(1-u+uv)}. \quad \text{(A3)}$$

(iii) For $|z| \geq 1$, let us change the variables into $u = 1/|z| \in [0,1]$ and $v = \frac{|1-z|-|z|+1}{2} \in [0,1]$, this implies

$$dzd\bar{z} = \frac{8|z|^3|1-z|dudv}{|z-\bar{z}|} \qquad \frac{|1-z|}{|z|}|z-\bar{z}| = 4(1/u-1+2v)\sqrt{v(1-v)(1+uv)(1-u+uv)}. \tag{A4}$$

One gets

$$A(r,x_{\mathbb{P}}) = \int_0^1\int_0^1 \frac{2dudv}{u(1-u+2uv)\sqrt{v(1-v)(1+uv)(1-u+uv)}}\{u^2[S(rQ_s/u,x_{\mathbb{P}})S((1/u-1+2v)rQ_s,x_{\mathbb{P}}) - S(rQ_s,x_{\mathbb{P}})]^2 + [S(urQ_s,x_{\mathbb{P}})S((1-u+2uv)rQ_s,x_{\mathbb{P}}) - S(rQ_s,x_{\mathbb{P}})]^2\} \tag{A5}$$

which is easy to evaluate numerically, as this features only integrable singularities.

APPENDIX B: SMALL-β AND LARGE-Q^2 LIMIT OF $x_{\mathbb{P}}F_T^{q\bar{q}g}$

In this Appendix, we show that the small-β limit of the leading $\ln(Q^2)$ result $F_T^{q\bar{q}g}|_{LL(Q^2)}$ and the large-Q^2 limit of the leading $\ln(1/\beta)$ result $F_T^{q\bar{q}g}|_{LL(1/\beta)}$ coincide. The first case has been derived in the text and we obtained formula (26). We now show how, for $Q^2 \gg Q_s^2$, formulas (23) and (24) give the same result.

The starting point is the transverse overlap function

$$\Phi_T(z,r;Q^2) = \frac{\alpha_{em}N_c}{2\pi^2}\sum_f e_f^2([z^2+(1-z)^2]\varepsilon_f^2K_1^2(r\varepsilon_f) + m_f^2K_0^2(r\varepsilon_f)), \tag{B1}$$

where one can neglect quark masses with respect to Q^2. The z integration of (B1) can be done in the two limits $rQ \ll 1$ and $rQ \gg 1$: using the Mellin representation of $K_1^2(x)$, one gets

$$\int_0^1 dz[z^2+(1-z)^2]z(1-z)K_1^2[\rho\sqrt{z(1-z)}] = \sqrt{\pi}\int_{c-i\infty}^{c+i\infty}\frac{d\gamma}{2i\pi}\rho^{-2\gamma}\frac{\Gamma(\gamma-1)\Gamma(\gamma)\Gamma(\gamma+1)\Gamma(2-\gamma)\Gamma(4-\gamma)}{\Gamma(6-2\gamma)\Gamma(\gamma+1/2)} \quad 1<\mathrm{Re}(c)<2$$
$$= \frac{2}{3}\begin{cases} 4/\rho^4 & \text{for } \rho \gg 1 \\ 1/\rho^2 & \text{for } \rho \ll 1 \end{cases}. \tag{B2}$$

To obtain the second equality, we used the fact that in the $\rho \gg 1$ case ($\rho \ll 1$ case), the dominant contribution to the γ integration comes from the single pole at $\gamma = 2$ (at $\gamma = 1$). One can then write

$$\int_0^\infty rdr\int_0^1 dz\Phi_T(z,r;Q^2)f(r) = \frac{\alpha_{em}N_c}{3\pi^2}\sum_f e_f^2\left[\int_0^{2/Q}\frac{dr}{r}f(r) + 4\frac{1}{Q^2}\int_{2/Q}^\infty\frac{dr}{r^3}f(r)\right]. \tag{B3}$$

Note that in [28] a similar estimation was obtained. By contrast, the replacement $K_1(\rho) \to \Theta(1-\rho)/\rho$ was used and as a result, the normalization factors were not under control.

To complete the calculation, we need to compute $f(r) = A(r,x_{\mathbb{P}})$, in the two limits $rQ_s \ll 1$ and $rQ_s \gg 1$ (see [28]):

$$A(r,x_{\mathbb{P}}) = 2\pi r^2Q_s^2\int\frac{d\bar{r}}{\bar{r}^3}[2N(\bar{r},x_{\mathbb{P}}) - N^2(\bar{r},x_{\mathbb{P}})]^2 \quad \text{for } rQ_s \ll 1 \tag{B4}$$

$$A(r,x_{\mathbb{P}}) = 2\pi\ln(r^2Q_s^2)[1-N(rQ_s,x_{\mathbb{P}})]^2 \quad \text{for } rQ_s \gg 1. \tag{B5}$$

The first line is obtained from configurations in which the $q\bar{q}$ pair is small and is well separated from the gluon. When using those results in (B3) by dividing the r integration region in three domains, one sees that the dominant contribution comes from the region $r \in [2/Q, 1/Q_s]$. It is enhanced by the collinear factor $\ln(Q^2/Q_s^2)$:

$$x_{\mathbb{P}}F_T^{q\bar{q}g}(\beta=0,Q^2\gg Q_s^2) = \frac{C_FN_c\alpha_sQ_s^2\sigma_0}{6\pi^4}\sum_f e_f^2\ln\left(\frac{Q^2}{Q_s^2}\right)\int_0^\infty\frac{d\bar{r}}{\bar{r}^3}[2N(\bar{r},x_{\mathbb{P}}) - N^2(\bar{r},x_{\mathbb{P}})]^2. \tag{B6}$$

This formula is identical to formula (26).

[1] L. V. Gribov, E. M. Levin, and M. G. Ryskin, Phys. Rep. **100**, 1 (1983).

[2] E. Iancu, K. Itakura, and L. McLerran, Nucl. Phys. **A708**, 327 (2002).

[3] A. M. Staśto, K. Golec-Biernat, and J. Kwiecinski, Phys. Rev. Lett. **86**, 596 (2001).

[4] C. Marquet and L. Schoeffel, Phys. Lett. B **639**, 471 (2006).

[5] A. H. Mueller, Nucl. Phys. **B335**, 115 (1990); N. N. Nikolaev and B. G. Zakharov, Z. Phys. C **49**, 607 (1991).

[6] N. N. Nikolaev and B. G. Zakharov, Z. Phys. C **53**, 331 (1992).

[7] A. Bialas and R. Peschanski, Phys. Lett. B **378**, 302 (1996); **387**, 405 (1996); A. Bialas, R. Peschanski, and C. Royon, Phys. Rev. D **57**, 6899 (1998); S. Munier, R. Peschanski, and C. Royon, Nucl. Phys. **B534**, 297 (1998).

[8] K. Golec-Biernat and M. Wüsthoff, Phys. Rev. D **59**, 014017 (1998).

[9] K. Golec-Biernat and M. Wüsthoff, Phys. Rev. D **60**, 114023 (1999).

[10] J. Bartels, K. Golec-Biernat, and H. Kowalski, Phys. Rev. D **66**, 014001 (2002).

[11] E. Iancu, K. Itakura, and S. Munier, Phys. Lett. B **590**, 199 (2004).

[12] K. Golec-Biernat and S. Sapeta, Phys. Rev. D **74**, 054032 (2006).

[13] H. Kowalski, L. Motyka, and G. Watt, Phys. Rev. D **74**, 074016 (2006).

[14] G. Soyez, arXiv:0705.3672.

[15] Y. V. Kovchegov and L. D. McLerran, Phys. Rev. D **60**, 054025 (1999); **62**, 019901(E) (2000).

[16] I. Balitsky, Nucl. Phys. **B463**, 99 (1996); Phys. Lett. B **518**, 235 (2001); Yu. V. Kovchegov, Phys. Rev. D **60**, 034008 (1999); **61**, 074018 (2000).

[17] J. Jalilian-Marian, A. Kovner, A. Leonidov, and H. Weigert, Nucl. Phys. **B504**, 415 (1997); Phys. Rev. D **59**, 014014 (1998); J. Jalilian-Marian, A. Kovner, and H. Weigert, Phys. Rev. D **59**, 014015 (1998); E. Iancu, A. Leonidov, and L. McLerran, Nucl. Phys. **A692**, 583 (2001); Phys. Lett. B **510**, 133 (2001); E. Ferreiro, E. Iancu, A. Leonidov, and L. McLerran, Nucl. Phys. **A703**, 489 (2002); H. Weigert, Nucl. Phys. **A703**, 823 (2002).

[18] A. H. Mueller and A. I. Shoshi, Nucl. Phys. **B692**, 175 (2004); E. Iancu, A. H. Mueller, and S. Munier, Phys. Lett. B **606**, 342 (2005); A. H. Mueller, A. I. Shoshi, and S. M. H. Wong, Nucl. Phys. **B715**, 440 (2005); E. Iancu and D. Triantafyllopoulos, Nucl. Phys. **A756**, 419 (2005); Phys. Lett. B **610**, 253 (2005).

[19] S. Munier and R. Peschanski, Phys. Rev. Lett. **91**, 232001 (2003); Phys. Rev. D **69**, 034008 (2004); **70**, 077503 (2004).

[20] E. Iancu, Y. Hatta, C. Marquet, G. Soyez, and D. N. Triantafyllopoulos, Nucl. Phys. **A773**, 95 (2006).

[21] S. Chekanov *et al.* (ZEUS Collaboration), Eur. Phys. J. C **38**, 43 (2004).

[22] A. Aktas *et al.* (H1 Collaboration), Eur. Phys. J. C **48**, 749 (2006).

[23] C. Marquet, R. Peschanski, and G. Soyez, Nucl. Phys. **A756**, 399 (2005); Phys. Rev. D **76**, 034011 (2007); C. Marquet and G. Soyez, Nucl. Phys. **A760**, 208 (2005).

[24] M. Wüsthoff, Phys. Rev. D **56**, 4311 (1997).

[25] J. Bartels, H. Jung, and M. Wüsthoff, Eur. Phys. J. C **11**, 111 (1999).

[26] B. Kopeliovich, A. Schaefer, and A. Tarasov, Phys. Rev. D **62**, 054022 (2000).

[27] Y. V. Kovchegov, Phys. Rev. D **64**, 114016 (2001).

[28] S. Munier and A. Shoshi, Phys. Rev. D **69**, 074022 (2004).

[29] C. Marquet, Nucl. Phys. **B705**, 319 (2005); Nucl. Phys. **A755**, 603c (2005); K. Golec-Biernat and C. Marquet, Phys. Rev. D **71**, 114005 (2005).

[30] Y. V. Kovchegov, and E. Levin, Nucl. Phys. **B577**, 221 (2000).

[31] J. R. Forshaw, R. Sandapen, and G. Shaw, Phys. Lett. B **594**, 283 (2004).

[32] E. Levin and M. Wüsthoff, Phys. Rev. D **50**, 4306 (1994).

[33] A. Aktas *et al.* (H1 Collaboration), Eur. Phys. J. C **48**, 715 (2006).

[34] S. Chekanov *et al.* (ZEUS Collaboration), Nucl. Phys. **B713**, 3 (2005).

[35] S. Chekanov *et al.* (ZEUS Collaboration), Nucl. Phys. **B672**, 3 (2003); A. Aktas *et al.* (H1 Collaboration), Eur. Phys. J. C **50**, 1 (2007).

[36] C. Royon, L. Schoeffel, S. Sapeta, R. Peschanski, and E. Sauvan, Nucl. Phys. **B781**, 1 (2007).

[37] E. Gotsman, E. Levin, M. Lublinsky, U. Maor, and K. Tuchin, Phys. Lett. B **492**, 47 (2000); M. S. Kugeratski, V. P. Goncalves, and F. S. Navarra, Eur. Phys. J. C **46**, 413 (2006); H. Kowalski, T. Lappi, and R. Venugopalan, arXiv:0705.3047.

[38] M. Hentschinski, H. Weigert, and A. Schafer, Phys. Rev. D **73**, 051501(R) (2006); A. Kovner, M. Lublinsky, and H. Weigert, Phys. Rev. D **74**, 114023 (2006).